AIAA SciTech Forum
8–12 January 2018, Kissimmee, Florida
2018 AIAA Aerospace Sciences Meeting

10.2514/6.2018-1553

AIAA-2018-1553

Experimental Study of Serpentine Plasma Actuator for Transition to Turbulence

Arnob Das Gupta,[1] Alexander J. Lilley,[2] Aaron A. Dagen,[3] and Subrata Roy[4]
Applied Physics Research Group, University of Florida, Gainesville, Florida, 32608, USA

This paper presents the effect of square serpentine plasma actuator on a laminar developing boundary layer at a freestream velocity of 3 m/s. The ratio between the maximum mean velocity generated by the actuator in quiescent conditions to the freestream velocity is 0.017. The exposed electrode is powered using 18 kV_{pp} voltage signal running at 500 Hz with 2% duty cycle. The duty cycle was chosen to avoid immediate turbulization downstream of the actuator. The pinch and spread regions of the actuator create alternate thickening and thinning of the boundary layer by creating quasi streamwise vortices. The streaks formed downstream of the actuator, look like subharmonic sinuous streaks. This study provides additional experimental evidence to the previous numerical results on the transition mechanism promoted by the square serpentine plasma actuator.

I. Nomenclature

δ	=	boundary layer thickness thickness
δ^*	=	displacement thickness
γ	=	velocity ratio (ratio of mean velocity magnitude generated by the actuator to freestream velocity)
θ	=	momentum thickness
PIV	=	particle image velocimetry
Re_x	=	Reynolds number based on location on the plate and freestream conditions
SDBD	=	surface dielectric barrier discharge
TS	=	Tollmien-Schlichting
U_∞	=	freestream velocity of the wind tunnel
U_p	=	mean velocity magnitude of the plasma actuator in quiescent conditions

II. Introduction

THIS paper experimentally investigates the transition process created by a serpentine surface dielectric barrier discharge (SDBD) plasma actuator [1] when it trips an incoming laminar developing flow inside a rectangular channel. The prominence of SDBD actuators is mainly due to their ability to instantaneously (within milliseconds) generate wall jet in the desired direction by manipulating the electrical input signal. Also, they have no moving parts and are surface complaint, which is useful for near wall flow control. Various parameters can impact the performance of the SDBD actuator. These mainly include the geometry of the electrodes, frequency of operation, and amplitude or voltage of the input signal. Geometric modifications can result in better control authority of the flow [8] [9]. The standard linear SDBD actuators are known to promote TS wave transition [10]. A detailed study of the impact of frequency was recently studied by Benard et al. [11]. They showed that the driving frequency of the actuator interacts with the natural instabilities in the flow. The effect of voltage on the flowfield is more intuitive, since it increases the strength of the electric field across the actuator. This results in the increase in plasma wall-jet velocity which increases the impact on the flowfield.

Several experiments on plasma actuators have been conducted for controlling the transition to turbulence [2] [3]. The importance of geometry of the actuator has been presented by Hanson et al. [4]. They studied spanwise array

[1] Graduate Assistant, Mechanical and Aerospace Engineering (arnobdgupta@ufl.edu), AIAA student member.
[2] Undergraduate Assistant, Mechanical and Aerospace Engineering (alexlille@ufl.edu), AIAA student member.
[3] Undergraduate Assistant, Mechanical and Aerospace Engineering (adagen@ufl.edu), AIAA student member.
[4] Professor, Mechanical and Aerospace Engineering (roy@ufl.edu) AIAA Associate Fellow.

actuators with varied spacing to understand their impact on the flow field. The spanwise array actuators were first investigated by Roth, Sherman, and Wilkinson [5] to reduce drag on a flat plate. These actuators are known to create streamwise oriented vortices [6] which can be used to manipulate the low-speed streaks found in both transitional and fully developed turbulent flows. The impact of these vortices has been applied to several applications, including pitch and roll control, jet vectoring, circulation control, skin friction drag reduction, and vortex shedding control [7]

Recently Gupta and Roy [12] numerically studied the impact of a square serpentine SDBD actuator on a laminar flow and demonstrated that the transition mechanism was similar to an oblique wave transition [13]. Although this paper investigates flows of Reynolds number on the order of 10^4, relative to the Reynolds number of 10^5 for the numerical study, the qualitative findings can be applied to understand the effect of serpentine actuators on transitional flows. Particle image velocimetry is conducted to obtain the boundary layer variations at different locations. Flow visualizations are also performed to observe the structures generated or modified by the serpentine SDBD actuator.

The paper is structured as follows. In Section III the experimental setup is described along with the details on the square serpentine SDBD actuator. Section IV provides the results and discussion for the effect of square serpentine SDBD actuator on a laminar flow field. Finally, conclusions are drawn in Section V.

III. Experimental Setup

All the experiments are performed in a low-speed open-loop wind tunnel. The test section has a cross section of $152.4\,\text{mm} \times 50.8\,\text{mm}$ and the total length of the test section is 558.8 mm. A schematic of the wind tunnel is shown in Fig. 1. The streamwise (x – direction), wall-normal (y – direction), and spanwise directions (z – direction) are also shown in Fig. 1. The starting of the test section is set as the origin O. The plasma actuator is flush-mounted on the bottom plate ($y = 0$). The wind tunnel velocity is set to 3 m/s using an Omega HH-USD thermo-anemometer.

A. Image Processing

Two-dimensional particle image velocimetry (PIV) was used to make quantitative measurements of the actuator's effect on the flow. To calculate various flow parameters the PIV software used was PIVlab [14] which is a MATLAB based program. The wind tunnel is seeded with fog juice containing a 1:5 glycerin to water ratio by volume. A hand held 1W blue laser (465 nm) along with a cylindrical lens is used to generate a continuous sheet along to light up the seeding particles. The Phantom V7.3 high-speed camera is used to record the images. The camera takes 6688 frames per second with an exposure time of 147.3µs. Images are recorded over a period of 1.084 seconds with a resolution of 800×600 pixels. Measurements are conducted at two different xy – planes (a-a and b-b) and the center of the camera viewing window $(152.4\,\text{mm} \times 50.8\,\text{mm})$ is positioned at four different locations (1-1, 2-2, 3-3, and 4-4) along the streamwise direction as shown in Fig. 1. Flow visualization is also conducted at a downstream location with respect to the actuator on the xz and yz – planes. The flow visualization images are taken using a Nikon D90 camera with a 50mm lens.

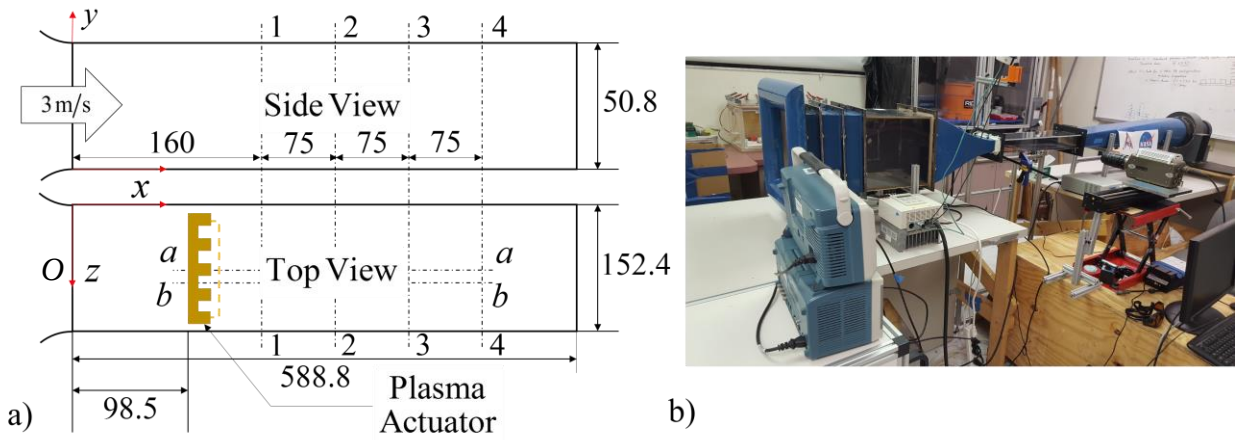

Fig. 1 Schematic of the test section of the low speed open loop wind tunnel. a) Line drawing of the test section and b) snapshot of the low speed wind tunnel. All dimensions are in mm.

B. Plasma Actuator Setup

The actuator design is depicted in Fig. 2. The input signal is created by a Tektronix AFG 3022B function generator which is amplified using a TREK 30/20A high-voltage power amplifier. The actuator electrodes are constructed using copper tape of 90 μm thickness. The dielectric material is acrylic with a thickness of 1.5 mm. The exposed electrode is powered using 18 kV_{pp} voltage signal running at 500 Hz with 2% duty cycle. The encapsulated electrode is grounded. The straight arrows shown in Fig. 2 depict the direction of plasma forces acting on the surrounding flowfield. The region where the arrows point towards each other is called the pinch region while the region where they point away from each other is called the spread region (ref. [8]). The plane *a-a* shown in Fig. 1 passes through the spread region and will be referred to as the spread plane while the plane *b-b* passes through the pinch region and will be referred as the pinch plane. The actuator also acts as a tripping device for the incoming laminar flow.

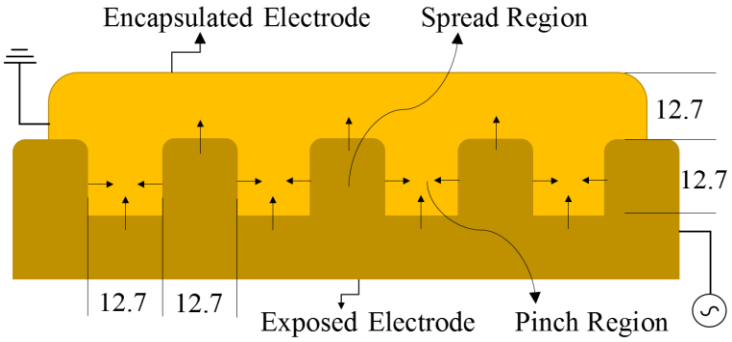

Fig. 2 Schematic of the square serpentine plasma actuator depicting the spread and pinch regions as well as the dimensions. All the dimensions are in mm.

IV. Results and Discussion

The incoming laminar boundary layer thickness was found to be 5.83 mm. The profile matches the Blasius boundary layer profile as shown in Fig. 3. The location corresponding to the boundary layer thickness gives a Reynolds number based on location on the flat plate, $\mathrm{Re}_x = 4.84\times10^4$. The momentum thickness at this location was $\theta = 6.714\times10^{-4}\,m$ and the shape factor, $H = 2.51$. These values indicate that the unperturbed flow is laminar inside the test section.

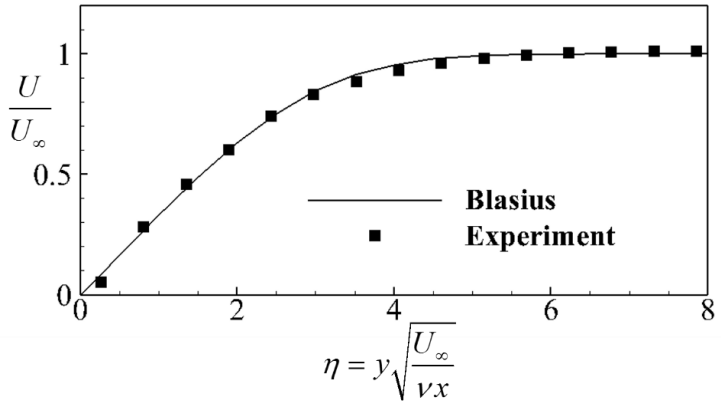

Fig. 3 Comparison of the incoming boundary layer profile with Blasius solution.

The plasma actuator is run in quiescent conditions to determine the mean velocity magnitude generated by the actuator. The velocity magnitude contour for the pinch plane *b-b* at the actuator location is shown in Fig. 4. It should be noted that the entire duration of the PIV lasted for 10 cycles of plasma actuation which did not allow the initial vortex to wash away.

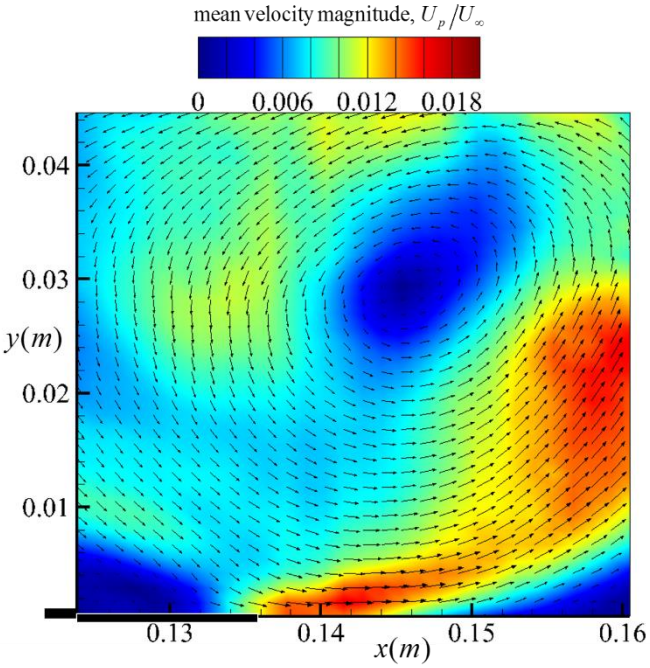

Fig. 4 Contour of normalized mean velocity magnitude generated by the actuator at the pinch plane.

The spatial variation in the wall-jet profile created by the actuator under quiescent condition is shown in Fig. 5. The maximum mean velocity magnitude occurs at 43.5 mm downstream of the actuator. The peak velocity is 1.7 % of the freestream velocity. This gives a velocity ratio, $\gamma = U_p/U_\infty = 0.017$. The low velocity ratio arises mainly due to the low duty cycle used for this study. The wall-normal location of the peak wall-jet velocity occurs at $y \approx 1.8\times10^{-3} m$ which is almost equal to the incoming boundary layer displacement thickness when the wind tunnel is on.

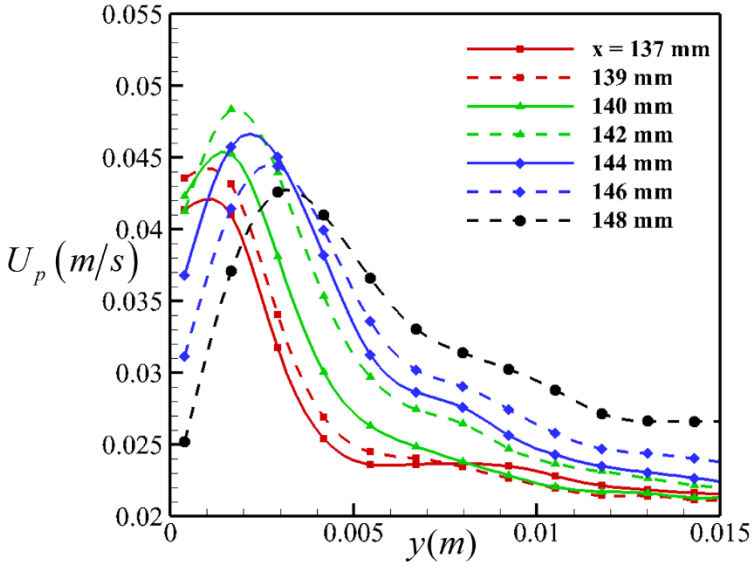

Fig. 5 Mean velocity magnitude generated by the plasma actuator at different locations downstream of the actuator pinch plane (*b-b* plane). Spline fit is through the data points to construct the lines.

The flow visualization of the effect of the actuator on the baseline flow is depicted in Fig. 6. The baseline case (plasma off) shows laminar streamline structures for both *xz* – plane. When the actuator is turned on these structures

get bundled together and create subharmonic sinuous streaks [15] as shown in Fig. 6 (c). This type of streaks was also observed in the numerical study by Gupta and Roy [12] as shown in Fig. 6 (e). It should be noted that this is only a qualitative comparison and that the numerical solution is for Re_x of the order 10^5 whereas the experiment has Re_x of the order 10^4. An implicit large eddy simulation was conducted for a single wavelength of the actuator operating in a compressible flow regime (Mach number = 0.5). The velocity ratio, γ was 10 %. The difficulty in matching the velocity ratio experimentally arose due to the reduction in velocity generated by the actuator when the frequency of actuation was lowered. Therefore, maintaining a specific velocity ratio while altering the frequency is a challenge when conducting experimental studies on actuators since both frequency and voltage can impact the wall jet velocity created by the actuator. Nonetheless, the experiment showed similar wavy subharmonic sinuous streaks (indicated in Fig. 6) downstream of the square serpentine actuator as observed numerically.

The spacing between the low speed streaks alternates and promotes the instability. When these streaks are viewed in the *yz* – plane small bulges are observed indicating a set of counter-rotating quasi streamwise vortices. The formation of these streaks by the plasma actuator happens downstream of the pinch region of the actuator. The bundling of the streaks results in alternate thickening and thinning of the boundary layer downstream of the actuator.

The numerical result shown in Fig. 6 (e) were obtained from solutions generated by Gupta and Roy [12]. They performed wall resolved implicit large eddy simulations to obtain the numerical results. The three-dimensional compressible Navier-Stokes equations were solved using discontinuous Galerkin method with third order accuracy in space and second order accuracy in time.

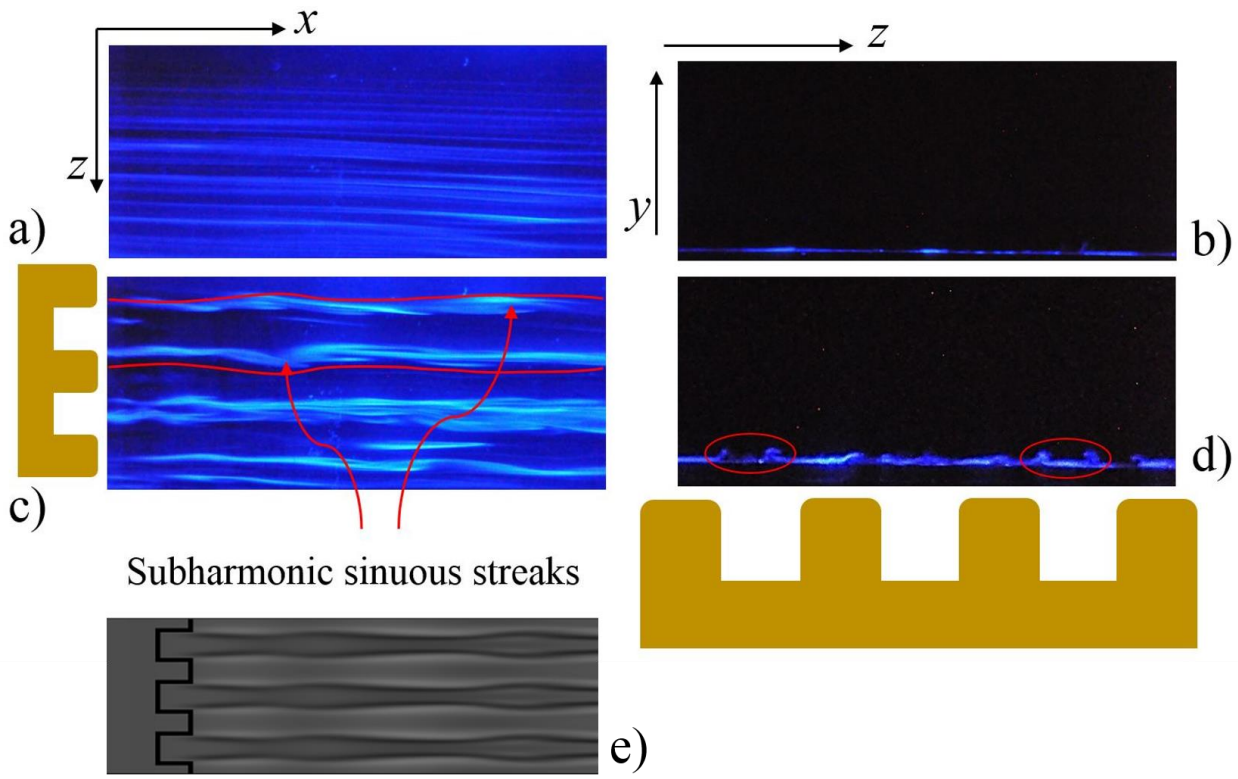

Fig. 6 Flow visualizations depicting the impact of square plasma actuator on streaks near the wall. Flow structures on the *xz* – plane for a) baseline and c) Plasma on case. Flow structures on the *yz* – plane for b) baseline and d) Plasma on case. e) Numerical solution for instantaneous velocity streaklines downstream of the serpentine actuator with the domain duplicated three times.

The boundary layer measurements depicted in Fig. 7 show that the velocities are not yet fully turbulent and are still in the transitional region. This is evident from the large differences in the boundary layer profile for the pinch (*a-a* plane) and spread (*b-b*) at the 3-3 location in Fig. 7 (b).The two locations shown correspond to 2-2 and 3-3 planes

(refer Fig. 1).The pinch regions increase the boundary layer thickness compared to the baseline, while the spread regions decrease the boundary layer thickness. This behavior becomes more prominent as the Reynolds number increases. All the velocity profiles show higher boundary layer thickness when compared with the Blasius laminar solution and smaller slope near the wall when compared to a $1/7^{th}$ power law profile. This is also an indication of the flow being in the transitional region.

V. Conclusion

Wind tunnel experiments were performed to understand the effect of square serpentine plasma actuator on a developing laminar boundary layer. The incoming laminar boundary layer is tripped using the actuator with a velocity ratio between the actuator and freestream of 1.7%. The flow visualization studies showed that the actuator bundles the streaklines downstream of the pinch region and the bundled streaklines behave similar to subharmonic sinuous streaks. This behavior was also observed by Gupta and Roy [12] and was concluded to be an oblique wave transition scenario. The boundary layer thickens downstream of the pinch region in comparison to the baseline, whereas it becomes thinner downstream of the spread region. However, further studies on the spanwise wavenumber and frequency are required to confirm this observation.

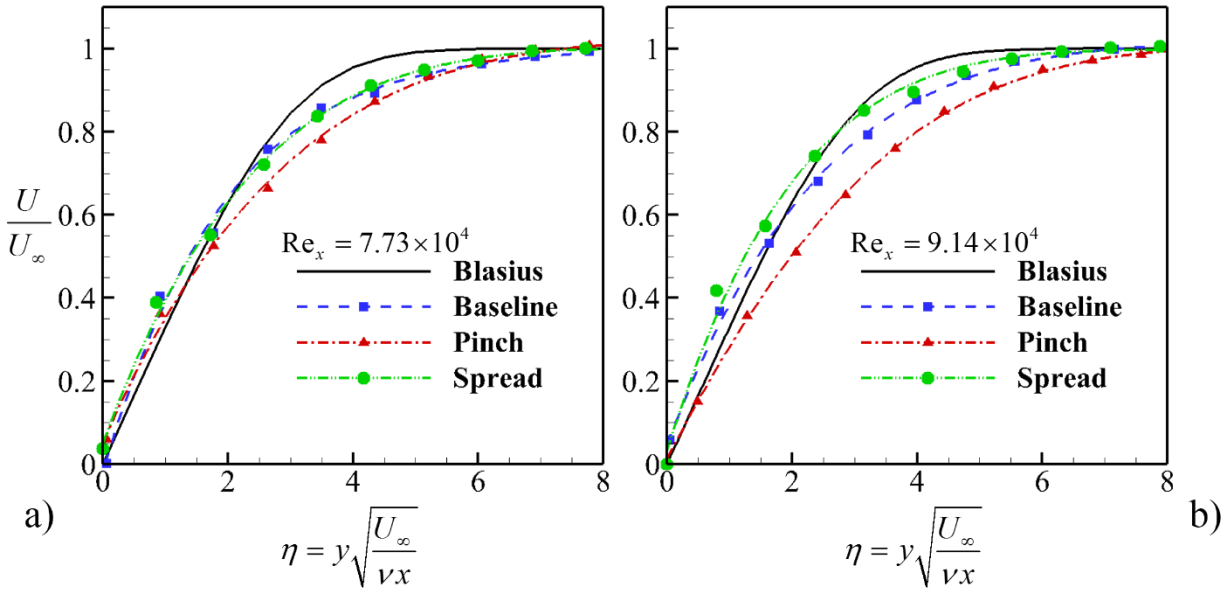

Fig. 7 Comparison of boundary layer profiles at two different locations in the streamwise direction. Boundary layer profiles at a) $\mathrm{Re}_x = 7.73\times10^4$ **(2-2 plane) and b)** $\mathrm{Re}_x = 9.14\times10^4$ **(3-3 plane). Smooth polynomial curves are fitted through the data points.**

Acknowledgments

This work was partially supported by AFOSR grant FA9550-15-1-0424 monitored by Drs. R. Ponnappan and Douglas Smith. We would also like to thank Mr. Stephen Wilkinson, NASA LaRC, for his advice regarding the experiments.

References

[1] Roy, S., and Wang, C. C., "Bulk flow modification with horseshoe and serpentine plasma actuators," *Journal of Physics D: Applied Physics*, vol. 42, no. 3, 2008, p. 030200,. https://doi.org/10.1088/0022-3727/42/3/032004

[2] Grundmann, S., and Tropea, C., "Active cancellation of artificially introduced Tollmien–Schlichting waves using plasma actuators," *Experiments in Fluids*, vol. 44, no. 5, 2008, pp. 795-806. https://doi.org/10.1007/s00348-007-0436-6

[3] Joussot, R., Weber, R., Leroy, A., and Hong, D., "Transition control using a single plasma actuator," *International Journal of Aerodynamics*, vol. 3, no. 1-2-3, 2013, pp. 26-46.

https://doi.org/10.1504/IJAD.2013.050912

[4] Hanson, R. E., Lavoie, P., Naguib, A. M., and Morrison, J. F., "Transient growth instability cancelation by a plasma actuator array," *Experiments in fluids*, vol. 49, no. 6, 2010, pp. 1339-1348. https://doi.org/10.1007/s00348-010-0877-1

[5] Roth, J. R., Sherman, D. M., and Wilkinson, S. P., "Electrohydrodynamic flow control with a glow discharge surface plasma," *AIAA Journal*, vol. 38, no. 7, 2000, pp. 1166-1172. https://doi.org/10.2514/2.1110

[6] Jukes, T. N., and Choi, K. S., "On the formation of streamwise vortices by plasma vortex generators," *Journal of Fluid Mechanics*, vol. 733, 2013, pp. 370-393. https://doi.org/10.1017/jfm.2013.418

[7] Wang, J. J., Choi, K. S., Feng, L. H., Jukes, T. N., and Whalley, R. D., "Recent developments in DBD plasma flow control," *Progress in Aerospace Sciences*, vol. 62, 2013, pp. 52-78. https://doi.org/10.1016/j.paerosci.2013.05.003

[8] Durscher, R. J., and Roy, S., "Three dimensional flow measurements Induced from serpentine plasma actuators in quiescent air," *Journal of Physics D: Applied Physics*, vol. 45, no. 3, 2012, pp. 035202-9. https://doi.org/10.1088/0022-3727/45/3/035202

[9] Caruana, D., Barricau, P., and Gleyzes, C., "Separation control with plasma synthetic jet actuators," *International Journal of Aerodynamics*, vol. 3, no. 1-2-3, 2013, pp. 71-83. https://doi.org/10.1504/IJAD.2013.050925

[10] Grundmann, S., and Tropea, C., "Experimental transition delay using glow-discharge plasma actuators," *Experiments in Fluids*, vol. 42, no. 4, 2007, pp. 653-657. https://doi.org/10.1007/s00348-007-0256-8

[11] Benard, N., Noté, P., Caron, M., and Moreau, E., " Highly time-resolved investigation of the electric wind caused by surface DBD at various ac frequencies," *Journal of Electrostatics*, vol. 88, 2017, pp. 41-48. https://doi.org/10.1016/j.elstat.2017.01.018

[12] Gupta, A. D, and Roy, S., "Three-dimensional plasma actuation for faster transition to turbulence," *Journal of Physics D: Applied Physics*, vol. 50, no. 42, 2017, p. 425201. https://doi.org/10.1088/1361-6463/aa8879

[13] Berlin, S., Lundbladh, A., and Henningson, D., "Spatial simulations of oblique transition in a boundary layer," *Physics of Fluids*, vol. 6, no. 6, 1994, pp. 1949-1951. https://doi.org/10.1063/1.868200

[14] Thielicke, W., and Stamhuis, E. J., "PIVlab – Towards User-friendly, Affordable and Accurate Digital Particle Image Velocimetry in MATLAB.," *Journal of Open Research Software*, vol. 2, no. 1, 2014 http://dx.doi.org/10.6084/m9.figshare.1092508

[15] Schoppa, W., and Hussain, F., "Coherent Structure generation in near-wall turbulence," *Journal of Fluid Mechanics*, vol. 453, 2002, pp. 57-108. https://doi.org/10.1017/S002211200100667X